Australia's National
Science Agency

GISERA | Gas Industry Social and Environmental Research Alliance

Baseline Seismicity of Beetaloo Basin-Interim Report 1

June 2023

Australian Government
Department of Industry, Science and Resources
Supported by Government of South Australia
Queensland Government
NORTHERN TERRITORY GOVERNMENT
origin
AUSTRALIA PACIFIC LNG
QGC
Santos

Citation

Saygin, E, Qashqai MT and Guo, P (2023) Baseline Seismicity of Beetaloo Basin. CSIRO, Australia.

Background

Hydraulic fracturing is a key enabling technology that helped unlock vast reserves of unconventional oil and gas resources within low permeability hydrocarbon rocks globally. The production takes place by injecting high pressure engineered fluids to create a permeable pathway for fluid flow in the subsurface. The injected fluids are generally disposed of at other wells for long term storage. It has been clearly demonstrated that (see Atkinson et al., 2020 for a comprehensive review) there is a correlation between hydraulic fracturing & injected water volumes and induced earthquake activity often in the vicinity of the production sites. The hydraulic fracturing is expected to create weak seismicity during opening of existing fractures to enhance permeability of the reservoir (also called operationally induced seismicity) (Atkinson et al., 2020). Larger and damaging earthquakes may occur if wastewater injection volumes are large enough, as in central Oklahoma in September 2016 (Pawnee event), where a magnitude 5.8 earthquake caused building damage. Hydraulic fracturing itself can trigger earthquakes in critically stressed faults as in the magnitude 5.7 event in Sichuan Basin, China. However, it must be noted that the lack of depleted reservoirs in the Northern Territory removes the possibility of large volumes of waste-water injection.

Beetaloo Sub-Basin is an onshore basin located in the Northern Territory, Australia, with a proven significant shale gas potential. In the case of prospective unconventional resource development activities, it is expected that hydraulic fracturing technologies will be used. A seismic monitoring plan is needed to distinguish between induced and baseline seismicity (natural earthquakes). Around the world, several seismic networks have been deployed and operated before, during and after the resource development operations. A good example is U.S. TexNet array, in which several seismographs are operated to provide real-time information about the seismic activity. In Australia, the Kimberley array has been deployed by the Geological Survey of Western Australia. CSIRO Scientists are analysing data from this array to quantify the baseline seismicity. Since late 2019, Geoscience Australia has been operating a six-element seismic broadband array in the Beetaloo Basin. The data is real-time telemetered to Geoscience Australia and freely open to the public (Figure 1D, blue triangles).

Outline

In this interim report, we present the locations of potential sources of seismic activity by mapping the available spatial data. We assessed the quality of the seismic stations operated by Geoscience Australia (Beetaloo Seismic Network – 2O) by analysing quarterly seismic noise variations, which is one of the parameters that determines the detection sensitivity of a seismic station. Next, we examined the waveforms recorded across the network for local, regional, and distant earthquakes. Using a state-of-the-art method, we detected and discriminated natural seismic activity within the region for December 2022. We detected several natural microseismic events during December, and the location of these events will be fine-tuned in the coming months. Finally, we present preliminary examples of ground motion simulations using a continent-scale seismic velocity model. We estimated the potential shaking in the future using parameters from a real earthquake that occurred in the nearby town of Tennant Creek.

Potential Sources of Seismic Activity

In this section, we first mapped the location of major roads, active mine sites, petroleum wells and also the current seismic network in Figure 1 to estimate the potential seismic source locations including anthropogenic sources such as vehicle noise from the road network (Figure 1A) and mine blasting (Figure 1B). The region is sparsely populated hence it is not expected to observe much traffic noise recorded by the seismic stations (Figure 1D). The large mining projects in the region to the north and south of the network generate observable seismic noise, where regular day time blasting by active mine sites in the area generates observable seismic signals, as has been previously reported by Geoscience Australia (Shamsalsadati et al., 2021).

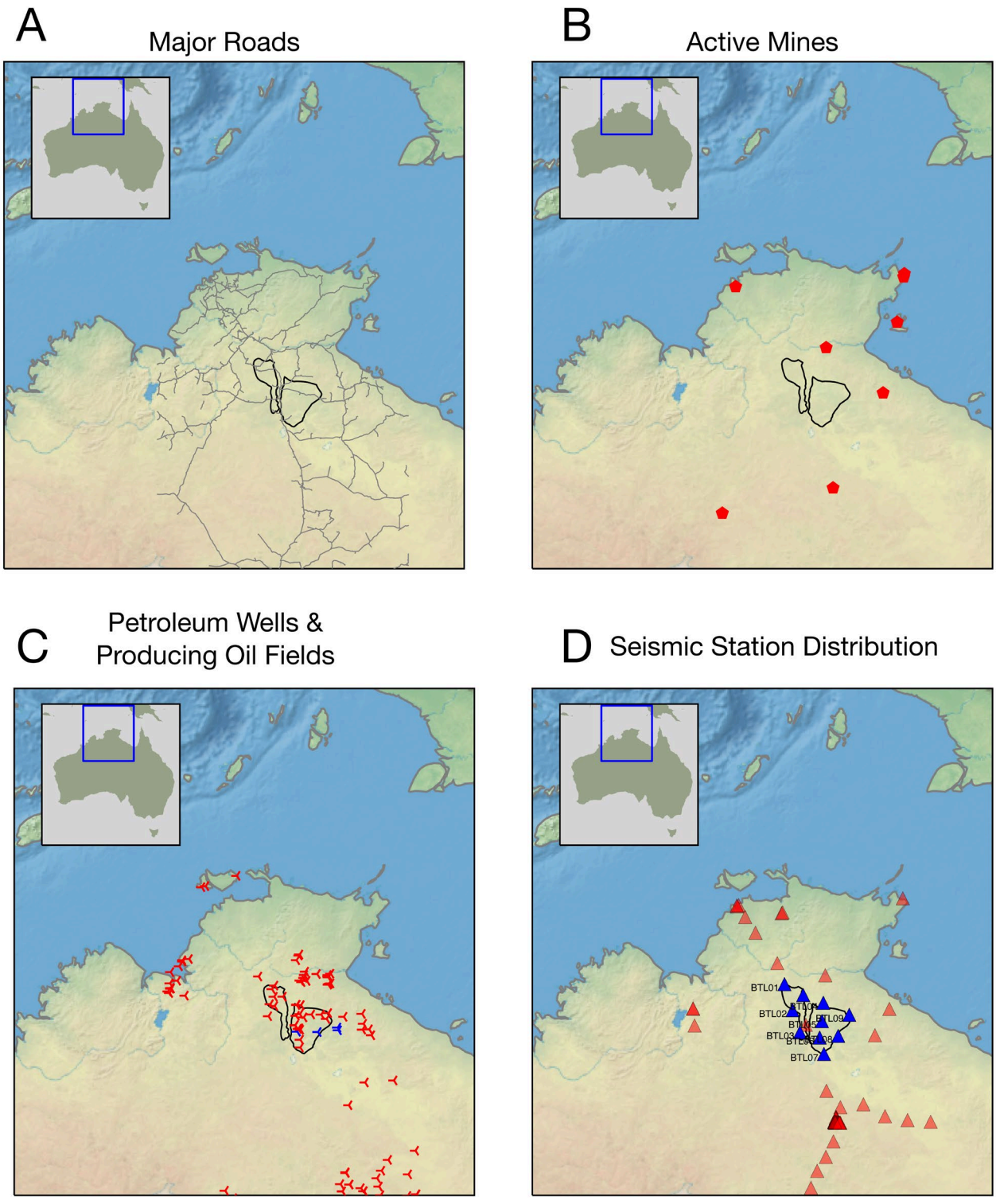

Figure 1 A) Location of major roads in the region, B) Distribution of active mine sites, C) Distribution of Petroleum wells (red) and producing oil fields (blue), D The distribution of current and past passive seismic stations. Red triangles show previous deployments, and blue triangles show the Beetaloo Seismic Network with station codes. The outline of the Beetaloo Basin is given with black line in each panel.

Performance of the Beetaloo Seismic Network

One common approach to quantifying the detection performance of seismic stations in the presence of surrounding noise, such as human activity and ocean-generated noise, is to conduct seismic noise analyses using continuous seismic records. These records capture various environmental sources, including ocean-ground interactions, anthropogenic sources (human-made), and very large earthquakes. Notably, the standing waves induced by storms in the ocean create a distinctive seismic signature in the frequency range of 0.09 – 0.18 Hz (Kennett, 2001). The level of noise variability also changes with seasonal variations in storm activity. Additionally, mid-continental stations generally exhibit lower noise levels, making them more sensitive to earthquake signals. Analysing these signals offers a metric for quantifying the theoretical performance of a seismic network (McNamara & Buland, 2004)

Background Seismic Noise Recorded at Beetaloo Seismic Network

We compute the probability density functions of seismic signals recorded at each station across the Beetaloo Basin Network to evaluate the range of variation of seismic noise in time and frequency. In the data processing, we remove the instrument response and digitiser gain to minimize the contribution of the instruments. The processing stream divides each record into one-hour-long segments with a 50% overlapping window. Then, we calculate the amplitude spectrum of each data segment and average them out to create the probabilistic density spectrum. We present the average variation of seismic noise levels as a function of frequency and time for three different seismic stations. Figures 2-4 provide quarterly changes in results for BTL01 (north of the basin), BTL05 (centre), and BTL07 (south of the basin).

Overall, the seismic noise levels are close to the 'New Low Seismic Noise Model' (McNamara & Buland, 2004) even at higher frequencies, indicating that the stations are located in quiet zones, which offer higher sensitivity to weak seismic activity, such as smaller magnitude earthquakes. Seismic noise generated by atmosphere-ocean-ground interactions, such as distant storms, often exhibits strong seasonality and slight interannual variability in Australia, as documented by Reading et al. (2014). However, in the case of the Beetaloo Seismic Network, we observed very little variation, as demonstrated by the computed probabilistic spectral density functions for the entire network.

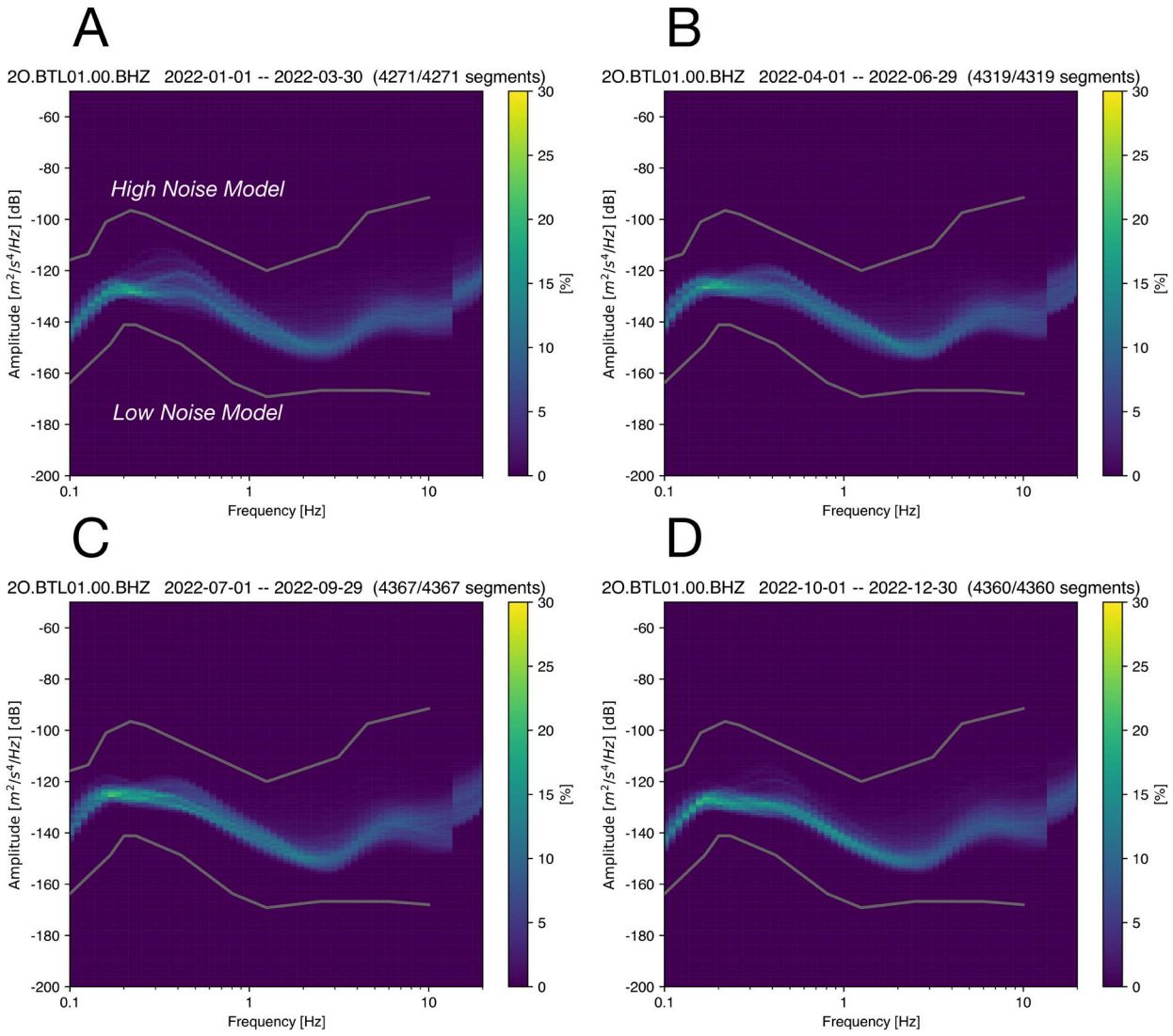

Figure 2 A) The background seismic noise variations for BTL01 (north) between January and March 2022 for signals between 0.1 and 50 Hz. B) April 2022 and June 2022. C) July 2022 and September 2022. D) October 2022 and December 2022. Although distant storm activities were expected to cause changes in lower frequencies (< 2 Hz), the observed signals remained close to the low noise model (as marked in A). The higher frequency signals were not greatly affected by expected anthropogenic activities.

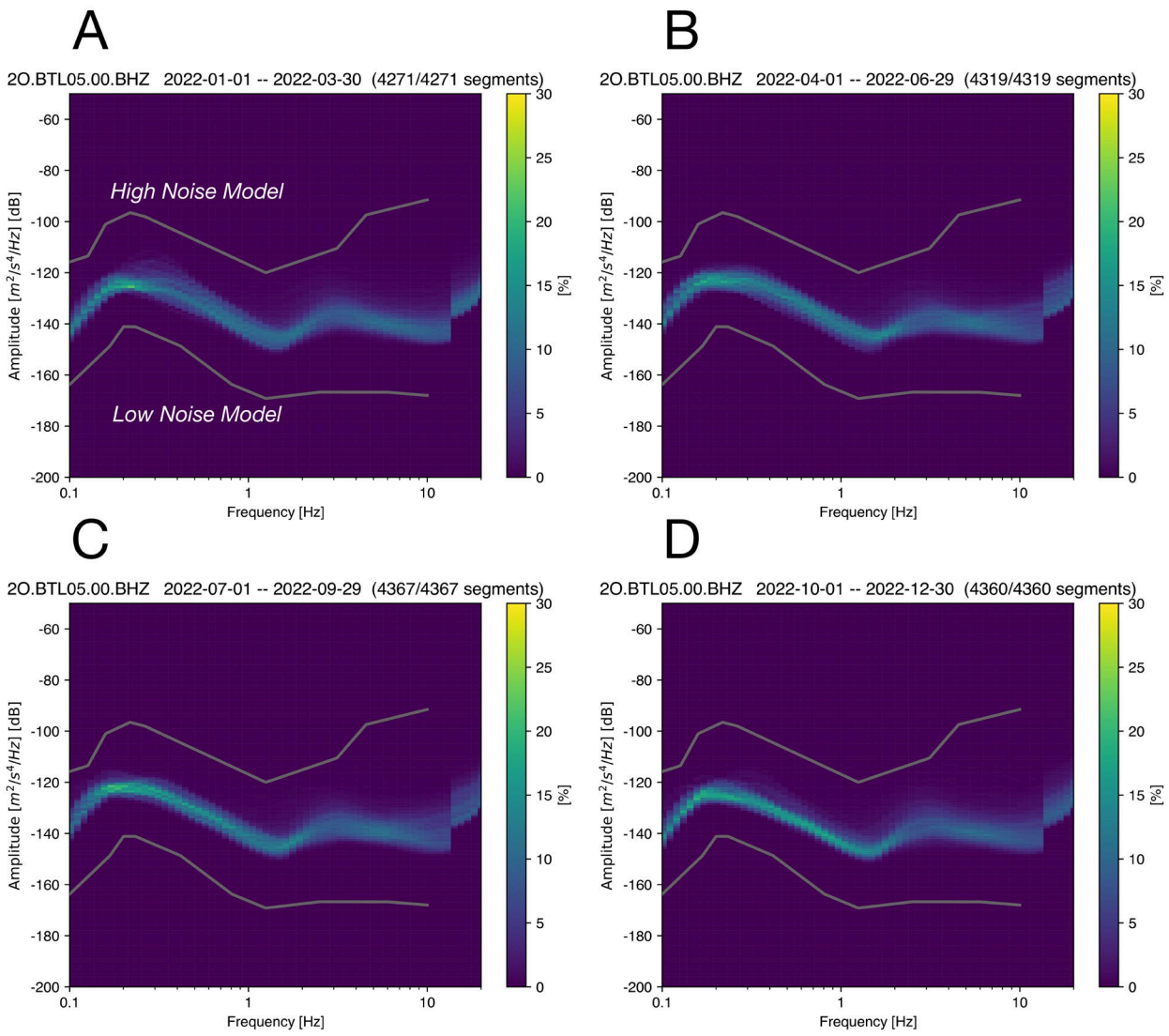

Figure 3: A) The background seismic noise variations for BTL05 (centre) between January and March 2022 for signals between 0.1 and 50 Hz. B) April 2022 and June 2022. C) July 2022 and September 2022. D) October 2022 and December 2022. Although distant storm activities were expected to cause changes in lower frequencies (< 2 Hz), the

observed signals remained close to the low noise model (as marked in A). The higher frequency signals were not greatly affected by expected anthropogenic activities.

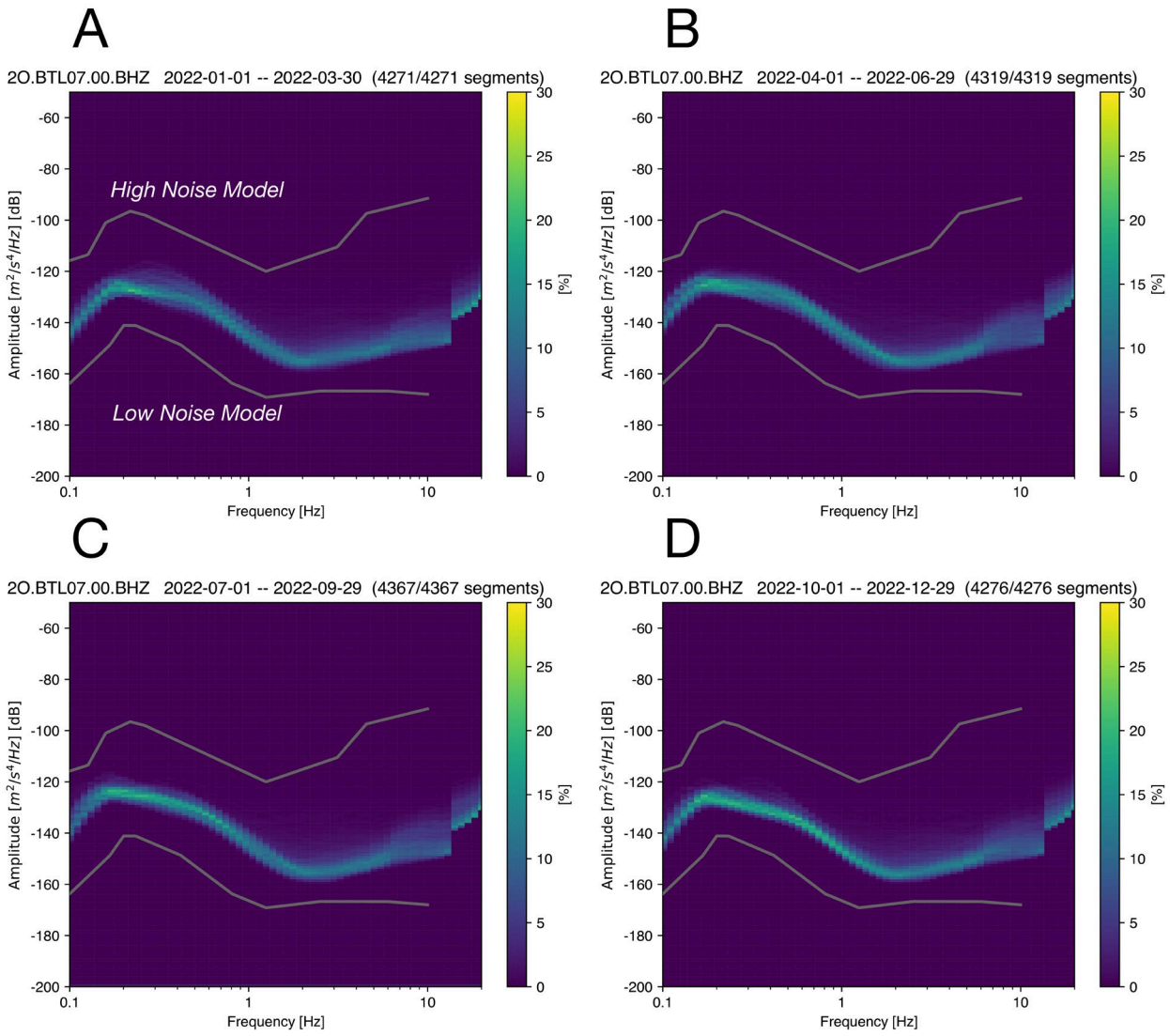

Figure 4: A) The background seismic noise variations for BTL07 (south) between January and March 2022 for signals between 0.1 and 50 Hz. B) April 2022 and June 2022. C) July 2022 and September 2022. D) October 2022 and December 2022. Although distant storm activities were expected to cause changes in lower frequencies (< 2 Hz), the observed signals remained close to the low noise model (as marked in A). The higher frequency signals were not greatly affected by expected anthropogenic activities.

Example Recordings of Distant Earthquakes

Another method to assess the performance of a seismic network involves examining recordings of medium to large magnitude regional and distant earthquakes catalogued by other agencies, such as the USGS. Various factors, including environmental noise, installation procedures, instrumentation, and site conditions, collectively influence the quality of the recorded signals, which subsequently affect the baseline seismic characterization efforts.

For our analysis, we selected three distinct earthquakes that occurred in 2022, originating from Australia, Indonesia, and Mexico, each with different magnitude. Figure 5 depicts the event locations and seismic station placements. Notably, despite a wide range of distances between the earthquakes and stations (~300 km – 14,000 km), the seismic events were captured with high fidelity across all three components (vertical, north-south, and east-west) of the stations, as shown in Figure 6. For instance, the wavefield resulting from the regional earthquake with a magnitude of 4.4 is clearly visible throughout the network (Figure 6C), indicating the interaction between the waves and the relatively shallow structure with high-frequency wave propagation. Conversely, the far-field earthquake originating from Mexico (Figure 6A) exhibits relatively weaker

waves originating from the deep layers of the Earth. Here, the Earth acts as filter, leading to the attenuation of most high-frequency waves.

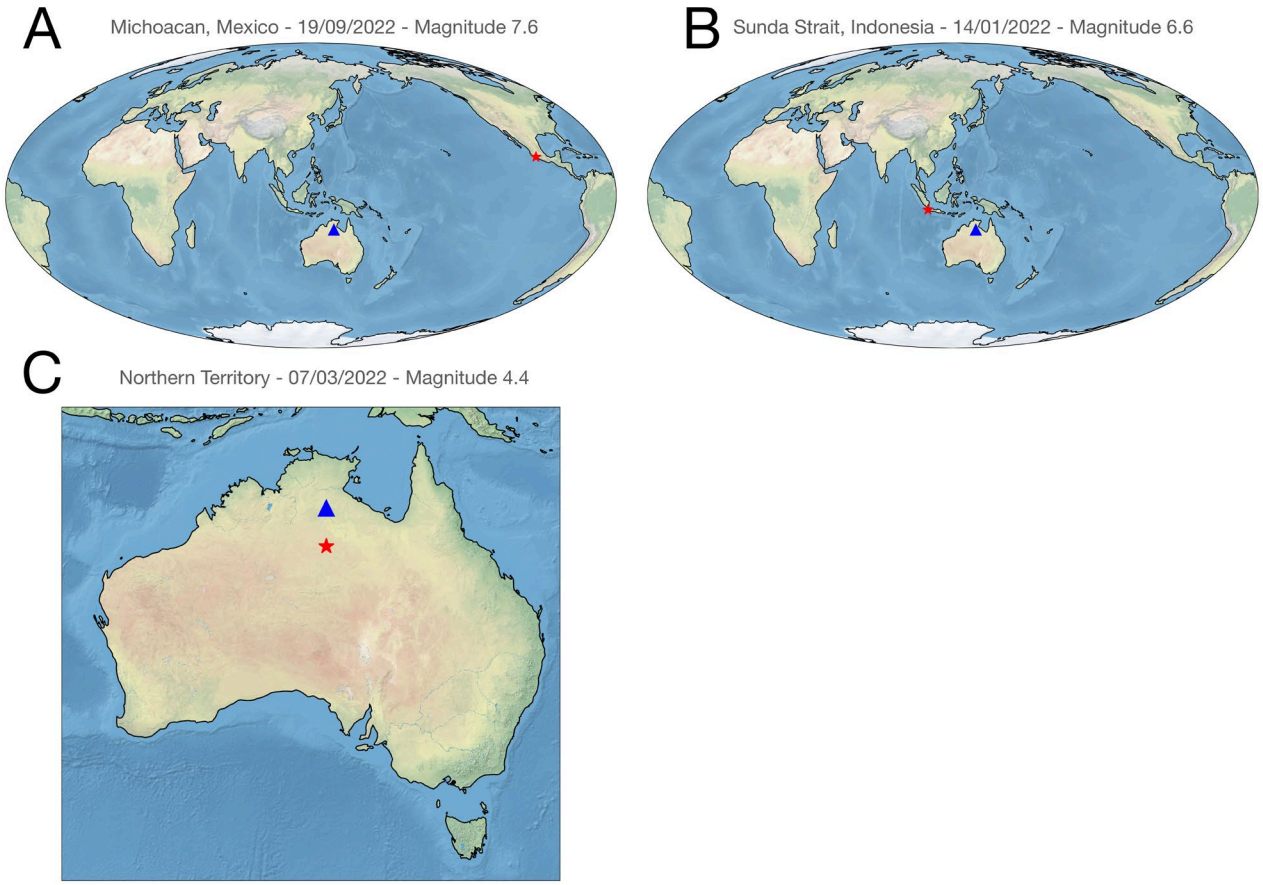

Figure 5: The location of three different earthquakes (red stars) recorded by the Beetaloo Basin seismic network (blue triangle). The average distances between earthquakes and the network stations are A) 14,000 km, B) 3200 km and C) 300 km. Titles of each sub plot show the location, date, and the magnitude of each event.

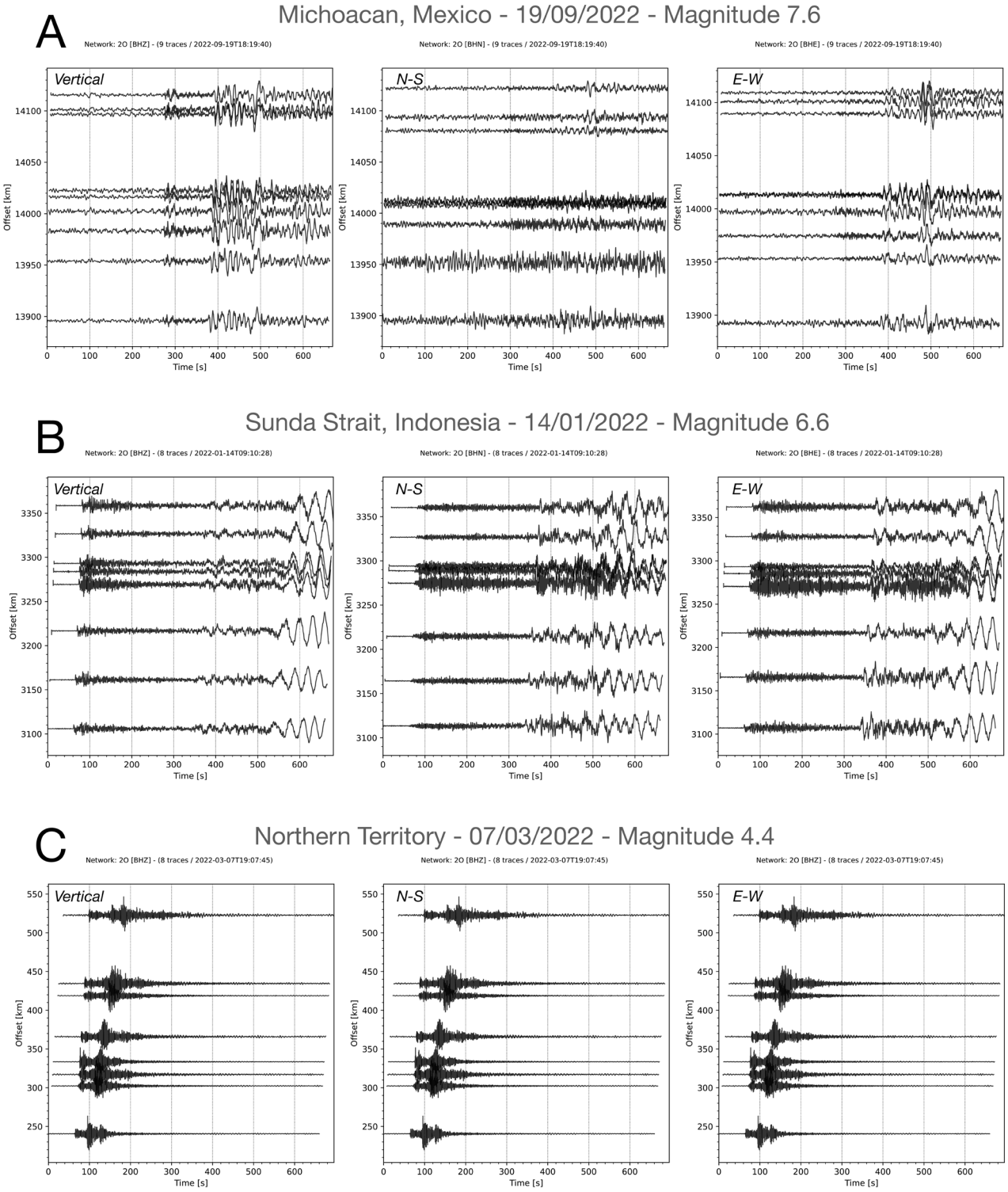

Figure 6: Three different earthquakes recorded by the Beetaloo Basin seismic network plotted for three components of the seismic sensor: vertical, north-south and east-west. The y-axis of each plot shows the distance between the earthquake and the station. A) Magnitude 7.7 Mexico earthquake. B) Magnitude 6.6 Sunda Strait, Indonesia earthquake. C) Magnitude 4.4 Northern Territory earthquake. Both the near and far-field earthquakes are clearly recorded by the seismic stations, showing the robustness of the sensors.

Baseline Seismic Detection & Location

Despite being one of the quietest zones in Australia (Figure 7), seismic activity does occur in the NT. For example, on January 22, 1988, three large earthquakes with magnitudes (Mw) 6.6, 6.3, 6.2 occurred within hours of each other in Tennant Creek, south of the Beetaloo Basin, and caused destruction. The aftershock activity of these events still continues today (Figure 8) following the expected pattern of reduced frequency and magnitude, typically conforming to a power law relationship known as Omori's law. Omori's law describes the decay of seismicity rate over time (Shearer, 2009).

However, the rest of the territory is relatively quiet, especially within the Beetaloo Basin.

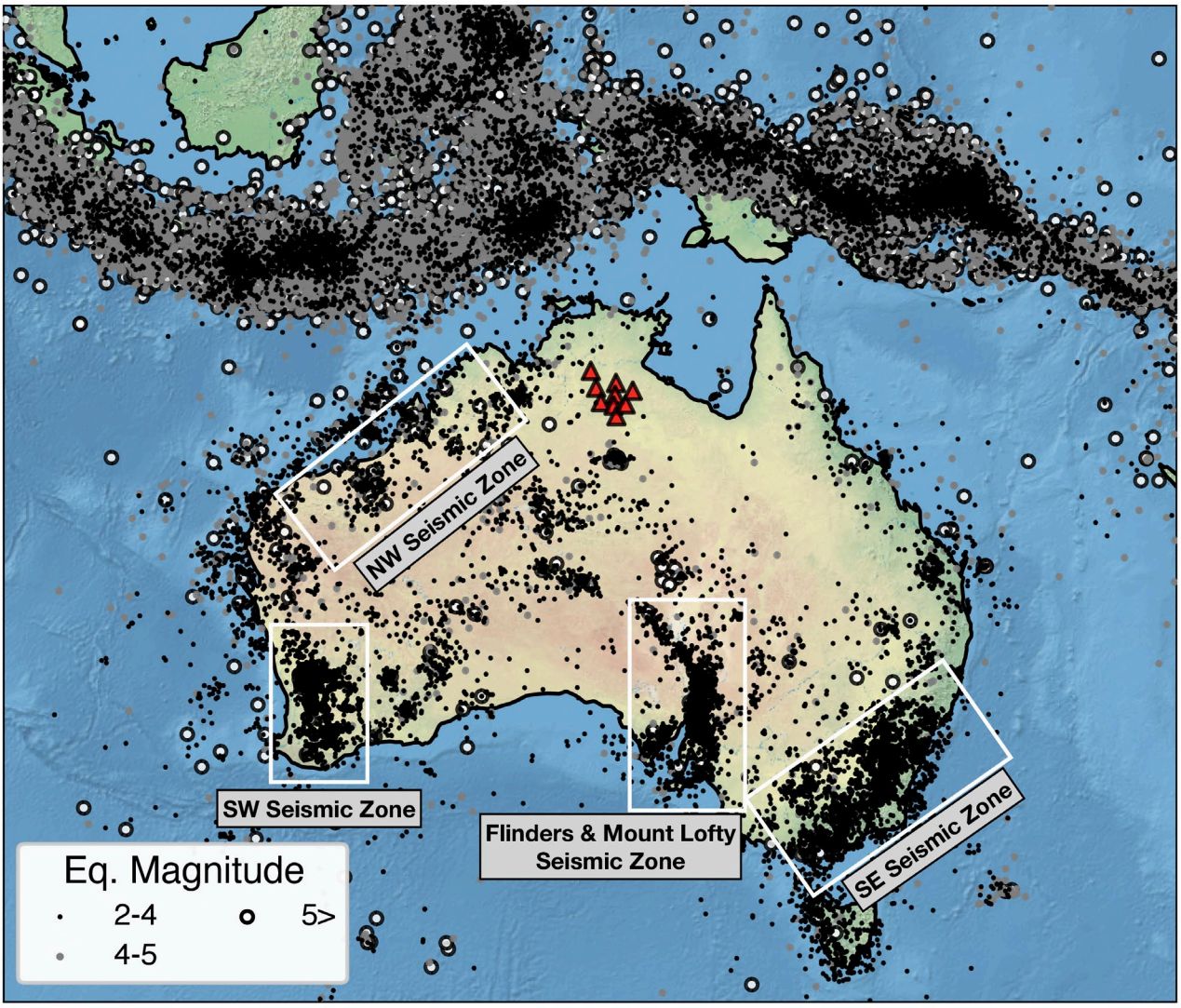

Figure 7: The distribution of earthquakes between 1900 and 2021 with magnitudes larger than 2 across the Australian continent. Four seismic zones are marked on the map. Modified from Rajabi et al. 2017. Source of the earthquakes: Geoscience Australia. Red triangles indicate the location of Beetaloo Seismic Network.

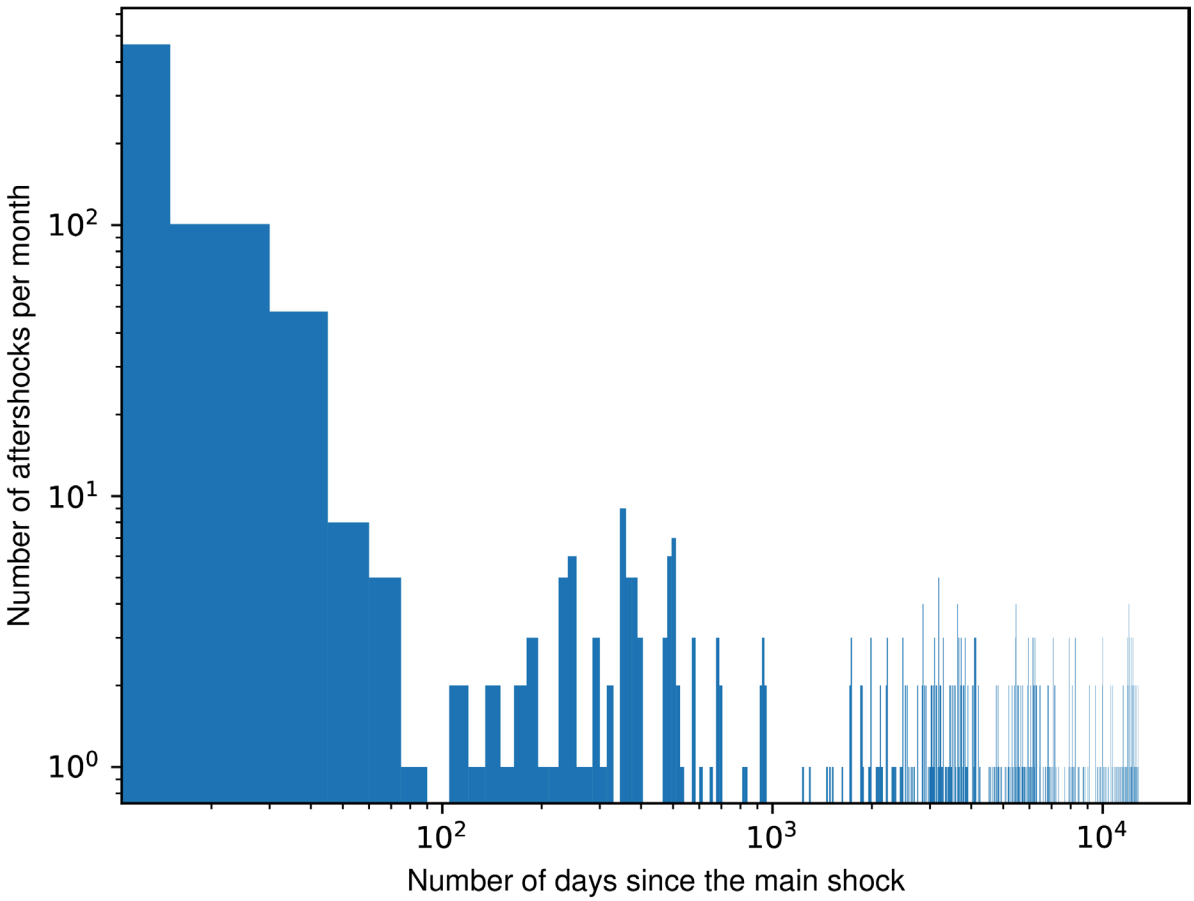

Figure 8 The aftershock distribution of 1988 Tennant Creek earthquakes. The distribution of the aftershocks shows a clear decay as expected following the Omori's Law. It is expected that the aftershocks will continue for another several decades.

We utilized the machine learning-based seismic detection algorithm developed by Mousavi et al. (2020) to analyse continuously recorded seismic data throughout December 2022. Through this analysis, we successfully identified more than 10 potential microseismic events exhibiting diverse seismic signal patterns. Figures 9-11 present plots of a subset of these events. Overall, the recorded signals demonstrate relatively weak yet coherent characteristics across multiple elements of the network for each event. The timing of these events suggests that their source cannot be attributed to anthropogenic activities, such as mining blasting, as most of them occurred later in the day. To further validate our findings, we cross-referenced the earthquake catalogues of both Geoscience Australia and USGS, but these events were not captured within their records.

The precise locations of these events, as well as future detections, will be determined in the subsequent stages of the project, following the complete integration of the seismic velocity model into the workflow.

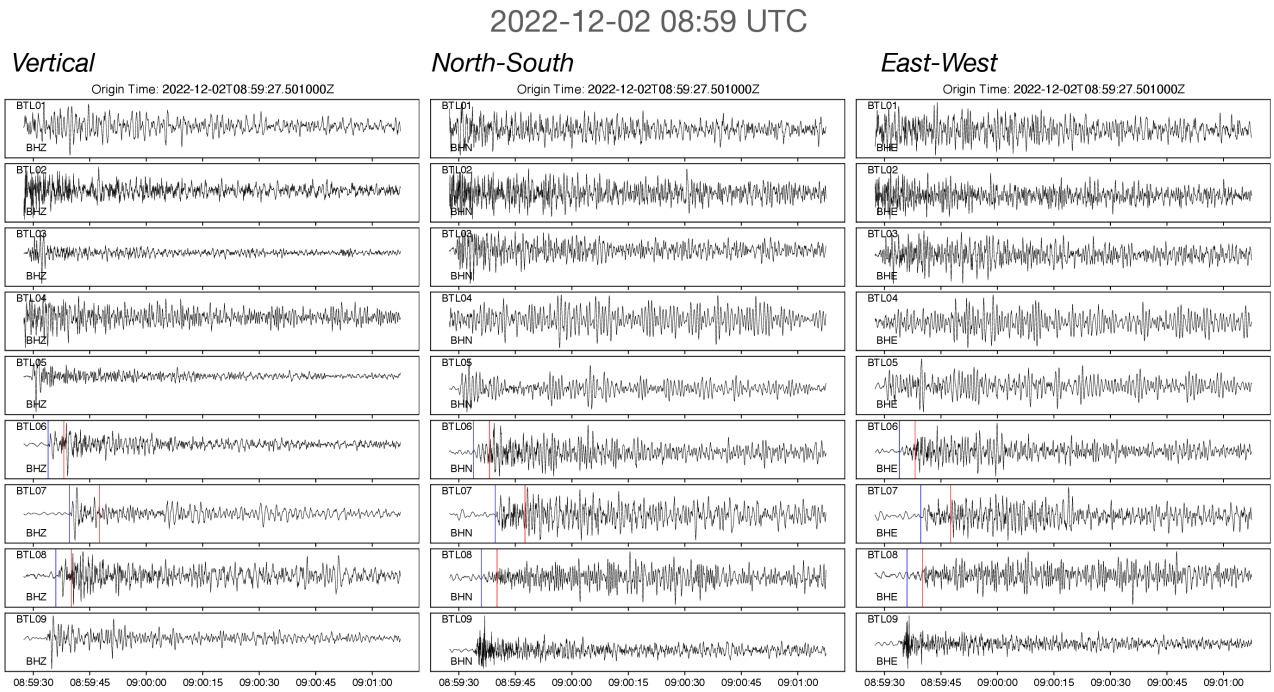

Figure 9: Example of earthquake detection on December 2, 2022. The coherence of waveforms and relative arrival differences at each station indicate a local/regional earthquake. The waveforms were filtered using a zero-phase Butterworth filter with a bandpass of 0.5-5 Hz.

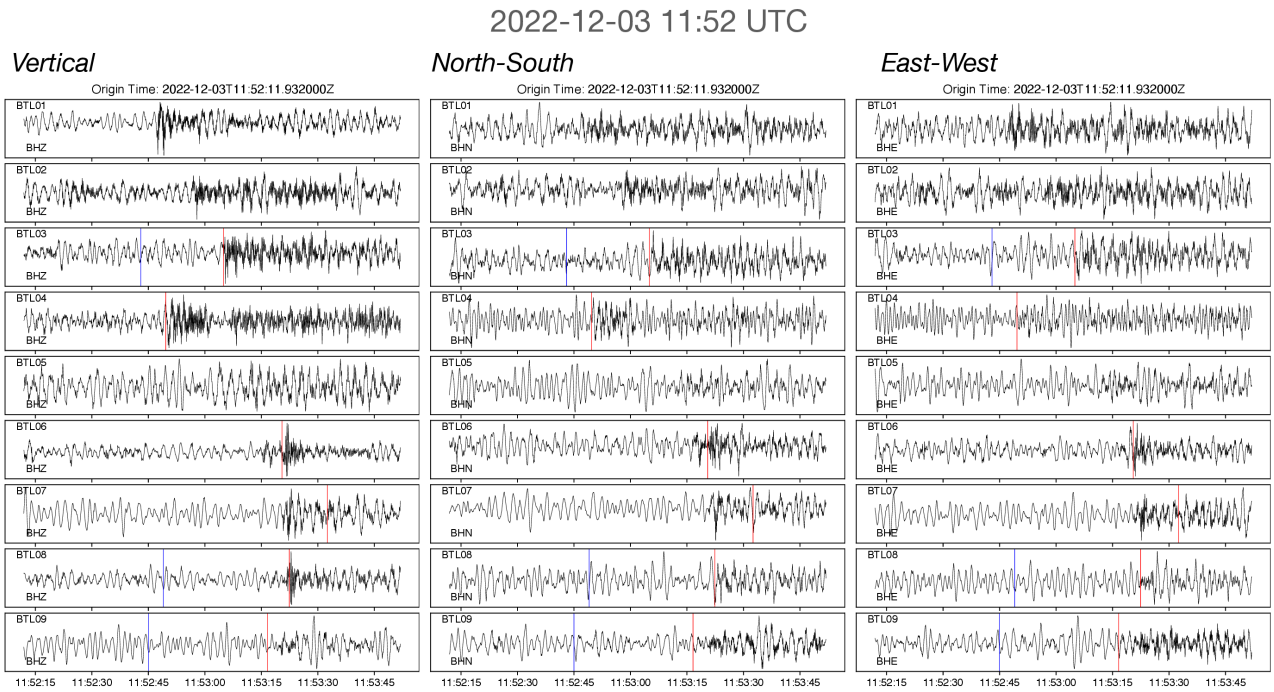

Figure 10: Example of earthquake detection on December 3, 2022. The coherence of waveforms and relative arrival differences at each station indicate a local/regional earthquake. The waveforms were filtered using a zero-phase Butterworth filter with a bandpass of 0.5-5 Hz.

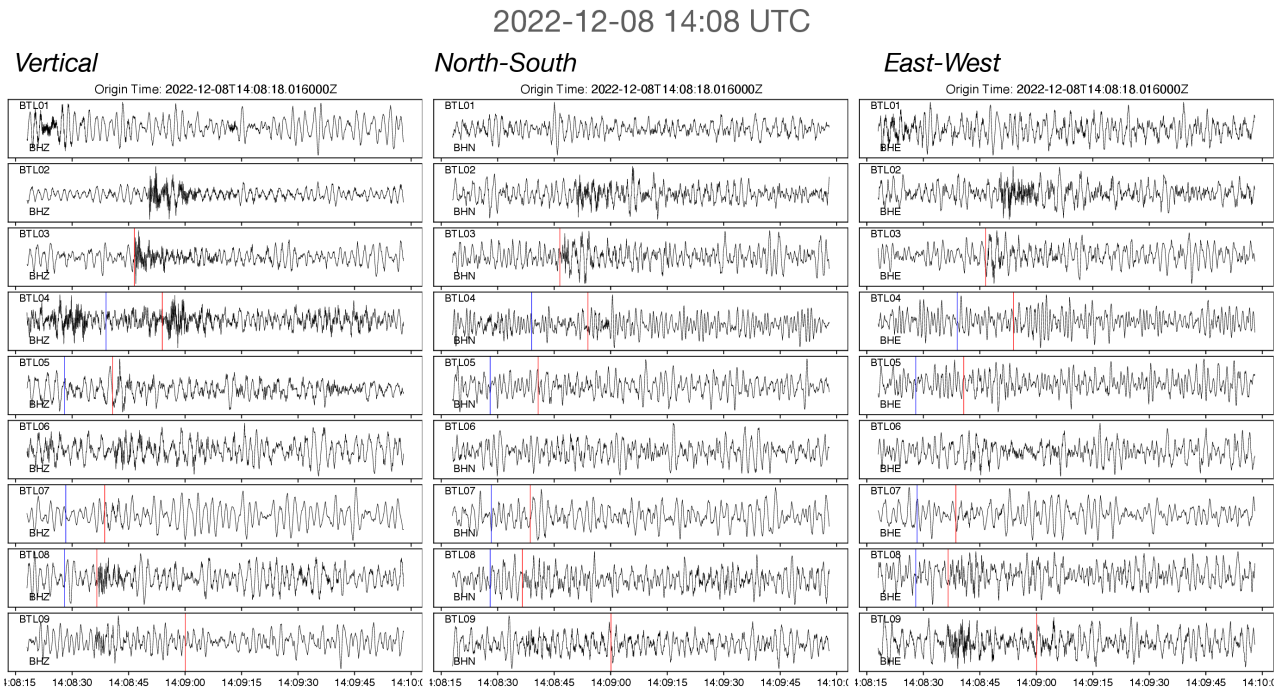

Figure 11: Example of earthquake detection on December 8, 2022. The coherence of waveforms and relative arrival differences at each station indicate a local/regional earthquake. The waveforms were filtered using a zero-phase Butterworth filter with a bandpass of 0.5-5 Hz.

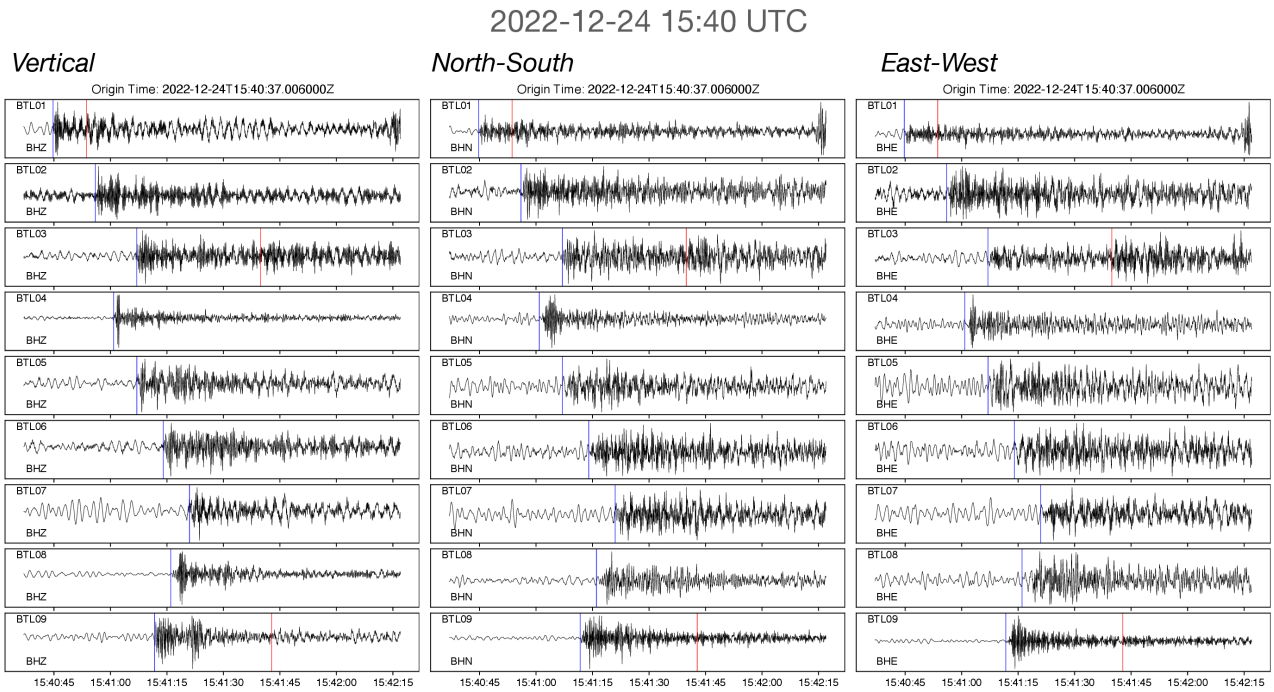

Figure 12: Example of earthquake detection on December 24, 2022. The coherence of waveforms and relative arrival differences at each station indicate a local/regional earthquake. The waveforms were filtered using a zero-phase Butterworth filter with a bandpass of 0.5-5 Hz.

Ground Motion Simulations

Ground motion simulations are frequently utilized to assess the physical impacts induced by earthquakes over extensive distances. The presence of diverse geological structures, particularly sedimentary basins, can significantly influence wavefield propagation, frequency content, and amplitudes.

One common approach to quantifying the effect of earthquakes on infrastructure, such as buildings and residential areas, is to simulate wave propagation within the Earth for a hypothetical yet realistic earthquake scenario. In this study, we simulate the wave propagation for an earthquake with a magnitude of 5.1 that occurred on August 1, 2019, at 01:22:16 (UTC), approximately 300 km south of the Beetaloo Seismic array.

For the calculations, we utilized the Open-source Seismic Wave Propagation Code (OpenSWPC) package (Maeda et al., 2017). OpenSWPC is a 3D/2D finite-difference-based, full elastic waveform simulator. Our calculations were performed in 3D using a source wavelet with a dominant frequency of 0.25 Hz. The moment tensor parameters for the simulation were based on the parameters of the 2019 event. Given the computational complexity of computing 3D wavefield propagation across a large area, we employed high-performance computing by distributing the computations across 256 cores (4 nodes). The numerical simulation was performed at CSIRO's in-house Petrichor supercomputer, which took approximately 20 minutes. The grid size is 0.5 km in both the x and y directions, and is 0.1 km in depth. The time step is 0.01 s. For the 3D simulation, there were 1200

and 1400 grid points in the x and y direction, and 200 grid points in depth. As for the Earth model, we constructed a representative model using the recent work of Chen et al. (2023). This model incorporated shear wave velocities obtained through continent-wide ambient seismic noise tomography. For the P-wave velocities, scaling factors were applied. The spatial resolution of this model is approximately 1 degree, while the depth resolution is around 5 km. Among the nearby stations, BTL07 and BTL06 exhibited relatively high-amplitude arrivals, which aligns with expectations as the seismic energy experienced comparatively less attenuation. However, BTL05, located in the centre of the basin, demonstrated a sudden increase in amplitude. This observation is attributed to the slowing down of seismic waves in the sedimentary basins, leading to an amplification of seismic wave amplitudes. Conversely, BTL04, the furthest station from the

simulated earthquake and outside the Beetaloo basin boundaries, exhibited the lowest amplitude (Figure 13 & 14).

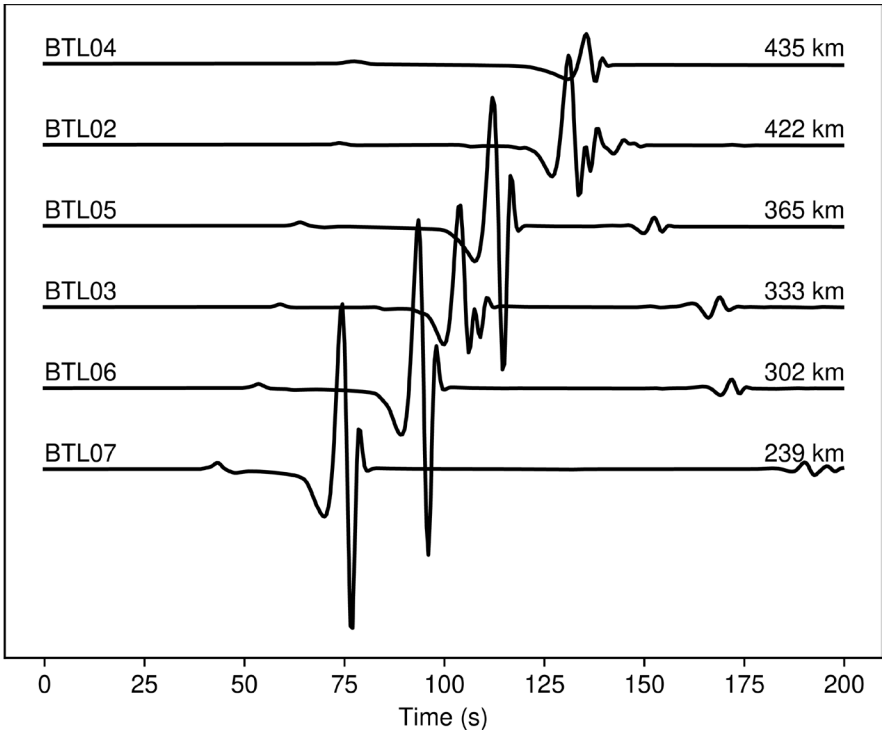

Figure 13 The simulated wavefield for the first 200 seconds of the 2019, 5.1 Tennant Creek earthquake. With increasing distance, more-complex wave trains can be observed across the network.

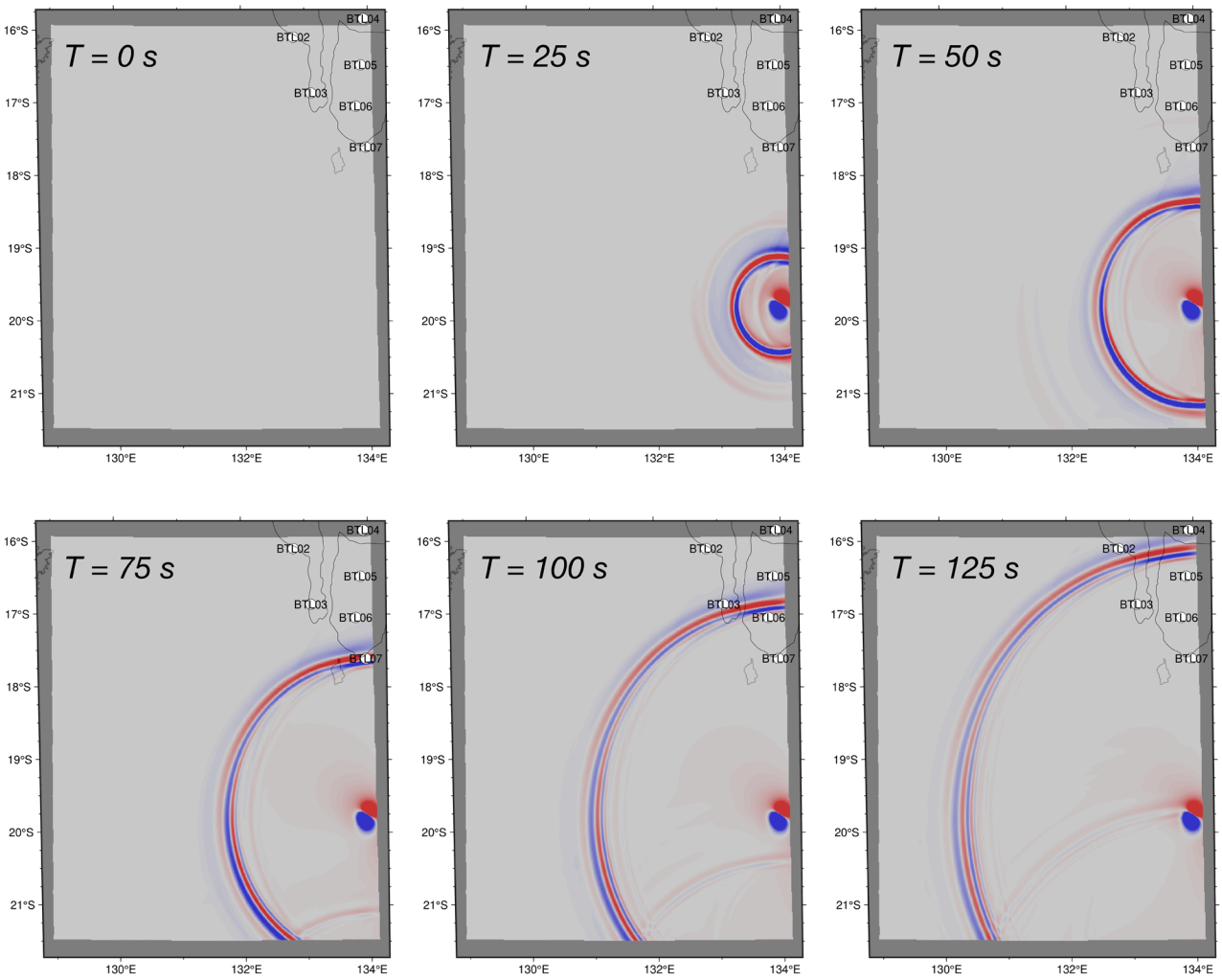

Figure 14 Snapshots of the computed wavefield between 0 - 125 seconds.

Summary

In this study, we assessed potential environmental noise sources in the region that could impact the detection performance of the seismic network. We examined the seasonal variations in noise levels across the network, which showed minimal changes, with overall seismic noise levels remaining below the high noise model.

Utilising a machine learning-based detector, we analysed the continuous data from December 2022 and successfully identified over 10 potential natural microseismic events that were not reported by earthquake monitoring agencies. Moreover, we integrated a recently developed 3D seismic-velocity model into our 3D waveform simulations to evaluate the influence of geological structure on expected natural seismicity.

In the next phase of the project, our focus will involve running the automatic detection algorithm on the remaining data and incorporating the unpublished dataset obtained from Geoscience Australia. Our primary objective will be to accurately locate the detected events in order to establish a baseline seismic catalogue. Additionally, we will further develop our physics-based ground motion modelling approach, expanding our analysis to include other earthquake scenarios.

References

Chen, Y., Saygin, E., Kennett, B., Qashqai, M. T., Hauser, J., Lumley, D., & Sandiford, M. (2023). Next-generation seismic model of the Australian crust from synchronous and asynchronous ambient noise imaging. Nature Communications, 14(1), 1192.

Kennett, B. L. N. (2001). The seismic wavefield: Volume 1, Introduction and Theoretical Development (Vol. 1). Cambridge University Press.

Maeda, T., Takemura, S., & Furumura, T. (2017). OpenSWPC: an open-source integrated parallel simulation code for modeling seismic wave propagation in 3D heterogeneous viscoelastic media (Vol. 69, pp. 1-20). Springer Berlin Heidelberg.

Mousavi, S. M., Ellsworth, W. L., Zhu, W., Chuang, L. Y., & Beroza, G. C. (2020). Earthquake transformer—an attentive deep-learning model for simultaneous earthquake detection and phase picking. Nature communications, 11(1), 3952. McNamara, D. E., & Buland, R. P. (2004). Ambient noise levels in the continental United States. Bulletin of the seismological society of America, 94(4), 1517-1527.

Rajabi, M., Tingay, M., Heidbach, O., Hillis, R., & Reynolds, S. (2017). The present-day stress field of Australia. Earth-Science Reviews, 168, 165-189.

Reading, A. M., Koper, K. D., Gal, M., Graham, L. S., Tkalčić, H., & Hemer, M. A. (2014). Dominant seismic noise sources in the Southern Ocean and West Pacific, 2000–2012, recorded at the Warramunga Seismic Array, Australia. Geophysical Research Letters, *41*(10), 3455-3463.

Shamsalsadati S. Allen T. Çomoğlu M., and Glanville H. (2021). The Beetaloo sub-basin baseline seismic monitoring project—Phase 1 observations, Australian Earthquake Engineering Society 2021 Virtual Conference.

Shearer, P. M. (2009). Introduction to seismology. Cambridge University Press.

Acknowledgement

This research has been funded through CSIRO's Gas Industry Social and Environmental Research Alliance (GISERA) with contributions from the Australian Government's Department of Industry, Science, Energy and Resources. GISERA is a collaboration between CSIRO, Commonwealth, state and territory governments and industry established to undertake research on the impacts of onshore gas exploration and development on the environment, and the socio-economic costs and benefits. For information about GISERA's governance structure, projects and research findings visit https://gisera.csiro.au.

As Australia's national science agency and innovation catalyst, CSIRO is solving the greatest challenges through innovative science and technology.

CSIRO. Unlocking a better future for everyone.

Contact us

1300 363 400
+61 3 9545 2176
csiro.au

For further information

1300 363 400
gisera.csiro.au

GISERA is a collaboration between CSIRO, Commonwealth and state governments and industry established to undertake publicly-reported independent research. The purpose of GISERA is to provide quality assured scientific research and information to communities living in gas development regions focusing on social and environmental topics including: groundwater and surface water, greenhouse gas emissions, biodiversity, land management, the marine environment, and socio-economic impacts. The governance structure for GISERA is designed to provide for and protect research independence and transparency of research.